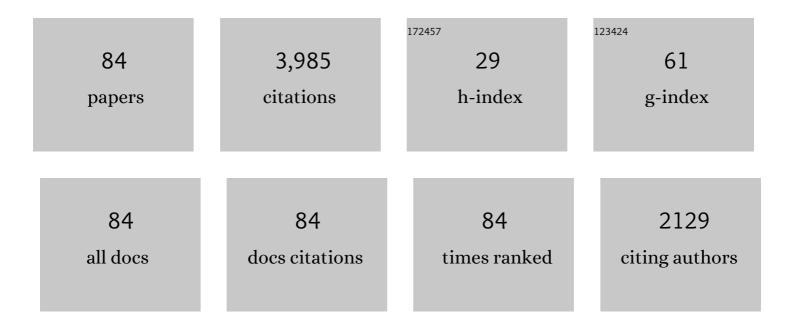
## Peter Stangeby

List of Publications by Year in descending order

Source: https://exaly.com/author-pdf/4076691/publications.pdf Version: 2024-02-01



#	Article	IF	CITATIONS
1	A full tungsten divertor for ITER: Physics issues and design status. Journal of Nuclear Materials, 2013, 438, S48-S56.	2.7	618
2	Physics basis and design of the ITER plasma-facing components. Journal of Nuclear Materials, 2011, 415, S957-S964.	2.7	361
3	Experimental divertor physics. Plasma Physics and Controlled Fusion, 1997, 39, 779-930.	2.1	349
4	Physics basis for the first ITER tungsten divertor. Nuclear Materials and Energy, 2019, 20, 100696.	1.3	307
5	Can detached divertor plasmas be explained as self-sustained gas targets?. Nuclear Fusion, 1993, 33, 1695-1705.	3.5	124
6	Basic physical processes and reduced models for plasma detachment. Plasma Physics and Controlled Fusion, 2018, 60, 044022.	2.1	124
7	Calculation of observable quantities using a divertor impurity interpretive code, DIVIMP. Journal of Nuclear Materials, 1992, 196-198, 258-263.	2.7	123
8	Far SOL transport and main wall plasma interaction in DIII-D. Nuclear Fusion, 2005, 45, 1589-1599.	3.5	123
9	Monte Carlo modelling of impurity ion transport for a limiter source/sink. Nuclear Fusion, 1988, 28, 1945-1962.	3.5	83
10	The Chodura sheath for angles of a few degrees between the magnetic field and the surface of divertor targets and limiters. Nuclear Fusion, 2012, 52, 083012.	3.5	77
11	Impurity retention by divertors. I. One dimensional models. Nuclear Fusion, 1995, 35, 1391-1412.	3.5	70
12	Interpretive modeling of simple-as-possible-plasma discharges on DIII-D using the OEDGE code. Journal of Nuclear Materials, 2003, 313-316, 883-887.	2.7	65
13	Modelling of beryllium erosion–redeposition on ITER first wall panels. Journal of Nuclear Materials, 2011, 415, S165-S169.	2.7	57
14	Electron pressure balance in the SOL through the transition to detachment. Journal of Nuclear Materials, 2015, 463, 533-536.	2.7	56
15	Influence of theE  —  Bdrift in high recycling divertors on target asymmetries. Plasma Physics Controlled Fusion, 2015, 57, 095002.	and 2.1	56
16	Impact of a narrow limiter SOL heat flux channel on the ITER first wall panel shaping. Nuclear Fusion, 2015, 55, 033019.	3.5	54
17	First experimental tests of a new small angle slot divertor on DIII-D. Nuclear Fusion, 2019, 59, 086054.	3.5	49
18	Obtaining reactor-relevant divertor conditions in tokamaks. Nuclear Fusion, 2011, 51, 063001.	3.5	47

#	Article	IF	CITATIONS
19	The inter-ELM tungsten erosion profile in DIII-D H-mode discharges and benchmarking with ERO+OEDGE modeling. Nuclear Fusion, 2017, 57, 056034.	3.5	47
20	Strong correlation between <i>D</i> <sub>2</sub> density and electron temperature at the target of divertors found in SOLPS analysis. Nuclear Fusion, 2017, 57, 056007.	3.5	44
21	Simulation of gross and net erosion of high-Z materials in the DIII-D divertor. Nuclear Fusion, 2016, 56, 016021.	3.5	41
22	SOLPS analysis of neutral baffling for the design of a new diverter in DIII-D. Nuclear Fusion, 2017, 57, 056043.	3.5	41
23	The magnitude of plasma flux to the main-wall in the DIII-D tokamak. Plasma Physics and Controlled Fusion, 2005, 47, 1579-1607.	2.1	40
24	A possible role of radial electric field in driving parallel ion flow in scrape-off layer of divertor tokamaks. Nuclear Fusion, 2007, 47, 762-772.	3.5	39
25	13C transport studies in L-mode divertor plasmas on DIII-D. Journal of Nuclear Materials, 2005, 337-339, 30-34.	2.7	38
26	ERO code benchmarking of ITER first wall beryllium erosion/re-deposition against LIM predictions. Physica Scripta, 2011, T145, 014008.	2.5	38
27	Identifying the location of the OMP separatrix in DIII-D using power accounting. Nuclear Fusion, 2015, 55, 093014.	3.5	35
28	Material migration studies with an ITER first wall panel proxy on EAST. Nuclear Fusion, 2015, 55, 023013.	3.5	35
29	Progress in the physics basis of a Fusion Nuclear Science Facility based on the Advanced Tokamak concept. Nuclear Fusion, 2014, 54, 073015.	3.5	33
30	Assessing material migration through 13C injection experiments. Journal of Nuclear Materials, 2011, 415, S278-S283.	2.7	30
31	Effects of divertor geometry and chemical sputtering on impurity behaviour and plasma performance in JET. Nuclear Fusion, 2000, 40, 379-396.	3.5	28
32	DIVIMP modeling of the toroidally symmetrical injection of 13CH4 into the upper SOL of DIII-D. Journal of Nuclear Materials, 2005, 337-339, 124-128.	2.7	27
33	Analysis for shaping the ITER first wall. Journal of Nuclear Materials, 2009, 390-391, 963-966.	2.7	26
34	Analysis of a tungsten sputtering experiment in DIII-D and code/data validation of high redeposition/reduced erosion. Fusion Engineering and Design, 2015, 94, 67-71.	1.9	25
35	A simple analytic model of impurity leakage from the divertor and accumulation in the main scrape-off layer. Nuclear Fusion, 2020, 60, 106005.	3.5	25
36	Interpretation of plasma impurity deposition probes. Analytic approximation. Physics of Fluids, 1987, 30, 3262.	1.4	24

#	Article	IF	CITATIONS
37	Transport and deposition of 13C from methane injection into partially detached H-mode plasmas in DIII-D. Journal of Nuclear Materials, 2007, 363-365, 72-77.	2.7	24
38	Dependence of neutral pressure on detachment in the small angle slot divertor at DIII-D. Nuclear Materials and Energy, 2019, 19, 487-492.	1.3	24
39	Interpretation of Langmuir, heat-flux, deposition, trapping and gridded energy analyser probe data for impure plasmas. Journal Physics D: Applied Physics, 1987, 20, 1472-1478.	2.8	23
40	Re-construction of detached divertor plasma conditions in DIII-D using spectroscopic and probe data. Journal of Nuclear Materials, 2005, 337-339, 256-260.	2.7	23
41	Net versus gross erosion of high- <i>Z</i> materials in the divertor of DIII-D. Physica Scripta, 2014, T159, 014030.	2.5	23
42	An experimental comparison of gross and net erosion of Mo in the DIII-D divertor. Journal of Nuclear Materials, 2013, 438, S309-S312.	2.7	22
43	Experimental validation of a model for particle recycling and tungsten erosion during ELMs in the DIII-D divertor. Nuclear Materials and Energy, 2018, 17, 164-173.	1.3	22
44	Overview of the recent DiMES and MiMES experiments in DIII-D. Physica Scripta, 2009, T138, 014007.	2.5	20
45	Measurements of net erosion and redeposition of molybdenum in DIII-D. Journal of Nuclear Materials, 2013, 438, S822-S826.	2.7	20
46	Impact of ELM control techniques on tungsten sputtering in the DIII-D divertor and extrapolations to ITER. Physics of Plasmas, 2019, 26, .	1.9	19
47	Evidence of near-SOL tungsten accumulation using a far-SOL collector probe array and OEDGE modelling in the DIII-D metal rings L-mode discharges. Nuclear Materials and Energy, 2019, 19, 287-294.	1.3	19
48	DiMES PMI research at DIII-D in support of ITER and beyond. Fusion Engineering and Design, 2017, 124, 196-201.	1.9	18
49	Utilization of outer-midplane collector probes with isotopically enriched tungsten tracer particles for impurity transport studies in the scrape-off layer of DIII-D (invited). Review of Scientific Instruments, 2018, 89, 101115.	1.3	18
50	Impurity transport at the plasma edge. Journal of Nuclear Materials, 1990, 176-177, 51-64.	2.7	17
51	OEDGE modeling of the DIII-D H-mode 13CH4 puffing experiment. Journal of Nuclear Materials, 2007, 363-365, 140-145.	2.7	17
52	Numerical assessment of the new V-shape small-angle slot divertor on DIII-D. Nuclear Fusion, 2021, 61, 116042.	3.5	17
53	SOLPS analysis of changes in the main SOL of DIII-D associated with divertor detachment vs attachment and closure vs openness. Nuclear Fusion, 2020, 60, 056011.	3.5	17
54	Far scrape-off layer and near wall plasma studies in DIII-D. Journal of Nuclear Materials, 2005, 337-339, 717-721.	2.7	15

#	Article	IF	CITATIONS
55	The roles of power loss and momentum-pressure loss in causing particle-detachment in tokamak divertors: I. A heuristic model analysis. Plasma Physics and Controlled Fusion, 2020, 62, 025012.	2.1	15
56	First evidence of dominant influence of E × B drifts on plasma cooling in an advanced slot divertor for tokamak power exhaust. Nuclear Fusion, 2021, 61, 054002.	3.5	15
57	Use of isotopic tungsten tracers and a stable-isotope-mixing model to characterize divertor source location in the DIII-D metal rings campaign. Nuclear Materials and Energy, 2019, 19, 358-363.	1.3	13
58	The roles of power loss and momentum-pressure loss in causing particle-detachment in tokamak divertors: II. 2 Point Model analysis that includes recycle power-loss explicitly. Plasma Physics and Controlled Fusion, 2020, 62, 025013.	2.1	13
59	Localized divertor leakage measurements using isotopic tungsten sources during edge-localized mode-y H-mode discharges on DIII-D. Nuclear Fusion, 2020, 60, 016028.	3.5	13
60	Modeling of ExB effects on tungsten re-deposition and transport in the DIII-D divertor. Nuclear Fusion, 2021, 61, 096018.	3.5	13
61	Manipulation of E×B drifts in a slot divertor with advanced shaping to optimize detachment. Nuclear Fusion, 2020, 60, 126030.	3.5	13
62	The role of divertor pumping in plasma detachment and particle exhaust in a closed divertor. Nuclear Fusion, 2021, 61, 016022.	3.5	13
63	The effect of thermo-oxidation on plasma performance and in-vessel components in DIII-D. Nuclear Fusion, 2013, 53, 073008.	3.5	11
64	A three-dimensional analytic model for discrete limiters in ITER. Nuclear Fusion, 2010, 50, 035013.	3.5	10
65	OEDCE modeling for the planned tungsten ring experiment on DIII-D. Nuclear Materials and Energy, 2017, 12, 755-761.	1.3	10
66	Measurements of tungsten migration in the DIII-D divertor. Physica Scripta, 2017, T170, 014041.	2.5	10
67	Modeling of inter- and intra-edge-localized mode tungsten erosion during DIII-D H-mode discharges. Nuclear Fusion, 2019, 59, 126018.	3.5	10
68	Evaluation of the impact of divertor closure on high-Z material transport and leakage in small angle slot divertor with toroidal tungsten rings in DIII-D. Physica Scripta, 2020, T171, 014072.	2.5	10
69	Indications of an inward pinch in the inner SOL of DIII-D from 13C deposition experiments. Journal of Nuclear Materials, 2009, 390-391, 376-379.	2.7	9
70	Control of high-Z PFC erosion by local gas injection in DIII-D. Journal of Nuclear Materials, 2015, 463, 605-610.	2.7	9
71	Plasma interactions with the outboard chamber wall in DIII-D. Journal of Nuclear Materials, 2009, 390-391, 785-788.	2.7	8
72	Experimental Advanced Superconducting Tokamak/material and plasma evaluation system material migration experiment. Physica Scripta, 2014, T159, 014069.	2.5	8

#	Article	IF	CITATIONS
73	Experimentally-based ExB drifts in the DIII-D divertor and SOL calculated from integration of Ohm's law using Thomson scattering measurements of Te and ne. Nuclear Materials and Energy, 2017, 12, 876-881.	1.3	8
74	Measurement and modeling of aluminum sputtering and ionization in the DIII-D divertor including magnetic pre-sheath effects. Nuclear Fusion, 2018, 58, 106019.	3.5	8
75	Comparison between SOLPS-4.3 and the Lengyel Model for ITER baseline neon-seeded plasmas. Nuclear Fusion, 2021, 61, 046029.	3.5	8
76	Measurements of gross erosion of Al in the DIII-D divertor. Journal of Nuclear Materials, 2015, 463, 810-813.	2.7	7
77	Reproduction of collector probe deposition profiles using the far-SOL impurity transport code 3DLIM. Nuclear Materials and Energy, 2020, 25, 100811.	1.3	6
78	The role of B <sub>T</sub> -dependent flows on W accumulation at the edge of the confined plasma. Nuclear Fusion, 2022, 62, 026037.	3.5	6
79	Developing solid-surface plasma facing components for pilot plants and reactors with replenishable wall claddings and continuous surface conditioning. Part A: concepts and questions. Plasma Physics and Controlled Fusion, 2022, 64, 055018.	2.1	6
80	Particle and parallel momentum balance equations with inclusion of drifts, for modelling strong- to weakly-collisional edge plasmas. Nuclear Fusion, 2006, 46, 975-993.	3.5	5
81	Characterizing Low-Z erosion and deposition in the DIII-D divertor using aluminum. Nuclear Materials and Energy, 2017, 12, 441-446.	1.3	5
82	Net versus gross erosion of silicon carbide in DIII-D divertor. Physica Scripta, 2020, T171, 014064.	2.5	5
83	Separatrix-to-Wall Simulations of Impurity Transport with a Fully Three-Dimensional Wall in DIII-D. Fusion Science and Technology, 2023, 79, 36-45.	1.1	1
84	Developing solid-surface plasma facing components for pilot plants and reactors with replenishable wall claddings and continuous surface conditioning. Part B: required research in present tokamaks. Plasma Physics and Controlled Fusion, 2022, 64, 055003.	2.1	0